Supporting Information

Ternary polythiophene enables over 17% efficiency organic solar cells

Qi Ai, Zhihui Lin, Xiangxi Wu, Yufan Zhu, Ke Wang, Xiaojun Li, Jianqi Zhang, Dan He, Yongfang Li and Fuwen Zhao*

1. General characterization

^{1}H NMR and ^{13}C spectra were measured on a Bruker Avance-400 spectrometer. UV-vis absorption spectra were measured on a UV-2600 UV-vis Spectrophotometer (Shimadzu, Japan). Gel permeation chromatography was performed on an Agilent PL-GPC50 by using chloroform as eluent and polystyrene as the standard. GIWAXS measurements were conducted on an Xenocs-SAXS/WAXS system with an X-ray wavelength of 1.5418 Å and 0.2° as an incidence angle. Pilatus 300 K was used as a 2D detector. Cyclic voltammetry was done by using a Shanghai Chenhua CHI660C voltametric analyzer under argon in an acetonitrile solution of tetra-*n*-butylammonium hexafluorophosphate (0.1 M). A glassy-carbon electrode was used as the working electrode, a platinum-wire was used as the counter electrode, and a Ag/AgCl electrode was used as the reference electrode. All potentials were corrected against Fc/Fc_{+} redox couple (Fc represents ferrocene.). AFM was performed on a Dimension 3100 microscope (Veeco) by using tapping mode. The *J-V* curves were measured by using a Keithley 2450 source-measure unit in the nitrogen-filled glove box along the reverse scan direction from -0.2 V to 1 V at room temperature. The scan speed and dwell times were fixes at 0.02 V per step and 0 ms, respectively. The photocurrent was measured under AM 1.5G illumination at 100 mW cm^{-2} by using a 3A solar simulator (LSS-55, Lightsky Technology Co., Ltd.). Light intensity is calibrated with a standard photovoltaic cell equipped with a KG2 filter (certificated by the National Institute of Metrology). The EQE measurements of devices were carried out in the air with a solar cell spectral response measurement system (LST-QE, Lightsky Technology Co., Ltd.). The light intensity at each wavelength was calibrated by a standard single-crystal Si photovoltaic cell. The thickness of all films was measured by the Bruker Dektak-XT. Transient photocurrent (TPC) and transient photovoltage (TPV) measurements were carried out under 337 nm with a 3.5 ns pulse laser (160 μJ per pulse at 10 Hz) and halide lamps (150 W). Voltage and current dynamics were recorded on a digital oscilloscope (Tektronix MDO3102).

2. Materials

Unless stated otherwise, all solvents and chemical reagents were obtained commercially and used without further purification. All reactions dealing with air- or moisture-sensitive compounds were carried out by using standard Schlenk techniques. BTP-eC9, Y6 and L8-BO were purchased from Derthon Co.. 3-Thiophenecarbonitrile (compound **1**), 3,4-thiophenedicarbonitrile (compound **2**) and 2,5-bis(trimethylstannyl)thiophene (T-Sn) were purchased from Innochem Co. and SunaTech Inc.. Bis(2-butyloctyl)2,2'-(ethene-1,2-diyl)(*E*)-bis(5-bromothiophene-3-carboxylate) (**M1**) was synthesized according to the literature[1].

3. Synthesis

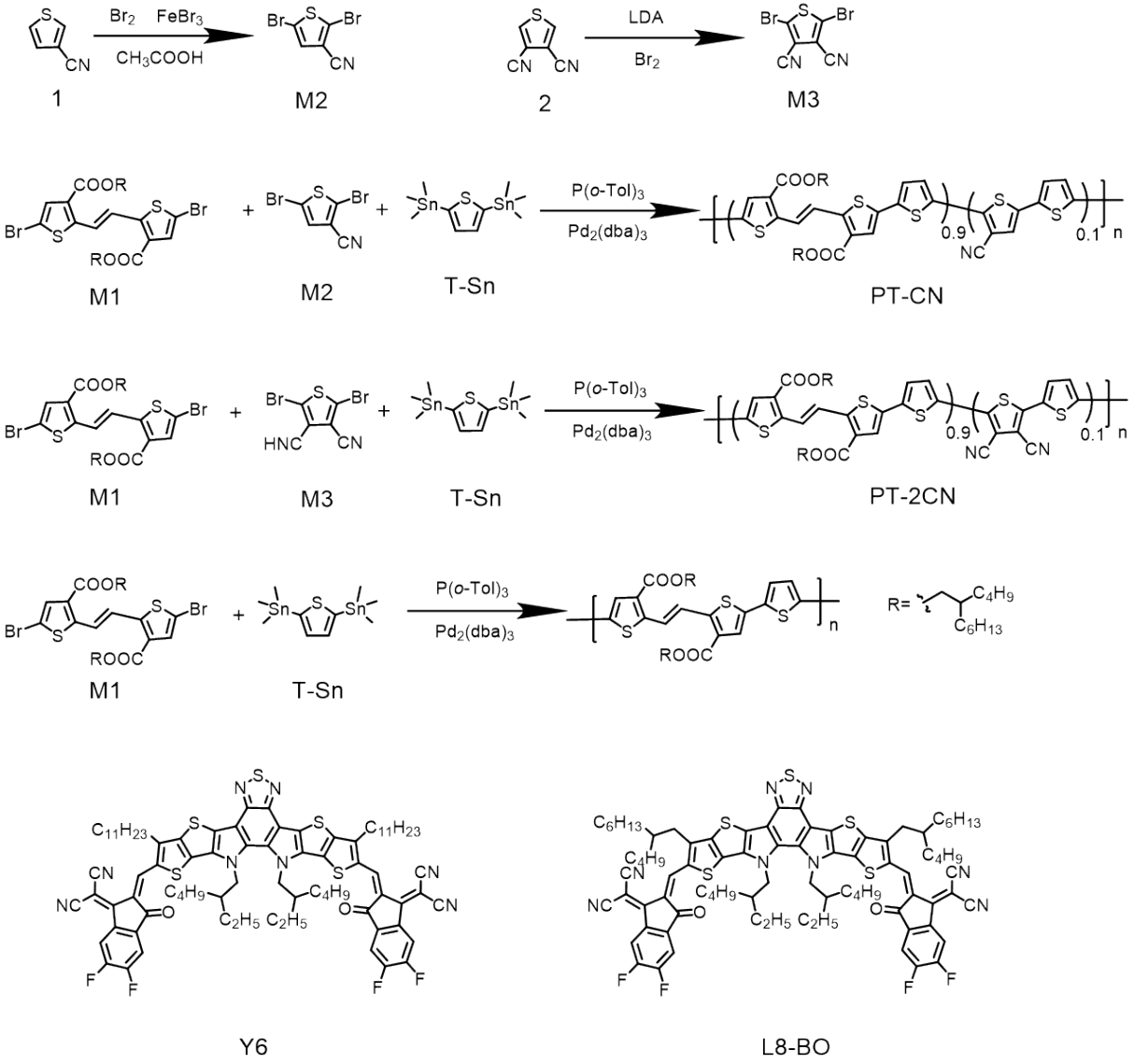

Scheme S1. The synthetic routes of PTVT-T, PT-CN and PT-2CN, and chemical structures of Y6 and L8-BO.

M1. M1 was synthesized according to the literature[1]. ^{1}H NMR ($CDCl_3$, 400 MHz, δ/ppm): 8.00 (s, 2H), 7.37 (s, 2H), 4.20 (d, J = 5.6 Hz, 4H), 1.75 (m, 2H), 1.45-1.14 (m, 32H), 0.89 (m, 12H).

2,5-dibromothiophene-3-carbonitrile (M2). To a solution of 3-cyanothiophene (200 mg, 1.83 mmol) and $FeBr_3$ (4.8 mg, 0.03 mmol) in dry $CHCl_3$ (6 ml) was added bromine (0.20 ml, 3.84 mmol) dropwise at 0 °C. The mixture was stirred under dark at room temperature overnight. Then it was poured into Na_2SO_3 aqueous solution and extracted with CH_2Cl_2 twice. The organic phase was dried over anhydrous Na_2SO_4 and filtrated. After the removal of solvent, the crude product was purified via column chromatography (silica gel) by using petroleum ether:CH_2Cl_2 (2:1) as eluent to give compound **M2** (470.2 mg, 97%). ^{1}H NMR ($CDCl_3$, 400 MHz, δ/ppm): 7.11 (s, 1H).

2,5-dibromothiophene-3,4-dicarbonitrile (M3). To a solution of 3,4-dicyanothiophene (200 mg, 1.49 mmol) in dry THF (8 ml) was added 2.0 M lithium diisopropylamide (LDA) (1.64

mL, 3.28 mmol) dropwise at -78 °C. After being stirred for 2 h, bromine (0.17 mL, 3.28 mmol) was added dropwise at the temperature. Then the mixture was stirred under dark at room temperature overnight and poured into Na_2SO_3 aqueous solution, following by extracted with CH_2Cl_2 twice. The organic phase was dried over anhydrous Na_2SO_4 and filtrated. After the removal of solvent, the crude product was purified via column chromatography (silica gel) by using petroleum ether:CH_2Cl_2 (1:1) as eluent to give compound **M3** (400.4 mg, 92%). ^{13}C NMR ($CDCl_3$, 100 MHz, δ/ppm): 124.60, 115.76, 110.30.

PTVT-T. To a mixture of compound **M1** (80 mg, 0.10 mmol), compound **T-Sn** (42.31 mg, 0.10 mmol), $Pd_2(dba)_3$ (2.84 mg, 0.003 mmol), P(*o*-Tol)$_3$ (9.45 mg, 0.031 mmol) in a Schlenk flask was added toluene (1.5 mL) under argon. The mixture was heated to reflux for 16 h. Then the solution was cooled to room temperature and added into methanol (150 mL) dropwise. The precipitate was collected and further purified via Soxhlet extraction by using methanol, hexane, CH_2Cl_2 and $CHCl_3$ in sequence. The $CHCl_3$ fraction was concentrated and added into methanol dropwise. The precipitate was collected and dried under vacuum overnight to give **PTVT-T** (56 mg, 78%). ^{1}H NMR ($CDCl_3$, 400 MHz, δ/ppm): 7.68-5.30 (br, aromatic protons), 4.27 (s, vinyl protons) 1.55-0.89 (br, aliphatic protons). M_n for **PTVT-T** is 25.6 kDa with a PDI of 2.51.

PT-CN. To a mixture of compound **M1** (80 mg, 0.10 mmol), compound **M2** (3.06 mg, 0.01 mmol), compound **T-Sn** (47.01 mg, 0.11 mmol) and $Pd_2(dba)_3$ (3.15 mg, 0.003 mmol) and P(*o*-Tol)$_3$ (10.50 mg, 0.024 mmol) in a Schlenk flask was added toluene (1.5 mL) under argon. The mixture was heated to reflux for 16 h. Then the solution was cooled to room temperature and added into methanol (150 mL) dropwise. The precipitate was collected and further purified via Soxhlet extraction by using methanol, hexane, CH_2Cl_2 and $CHCl_3$ in sequence. The $CHCl_3$ fraction was concentrated and added into methanol dropwise. The precipitate was collected and dried under vacuum overnight to give **PT-CN** (63 mg, 85%). ^{1}H NMR ($CDCl_3$, 400 MHz, δ/ppm): 7.52-7.00 (br, aromatic protons), 4.28 (s, vinyl protons), 1.55-0.88 (br, aliphatic protons). M_n for **PT-CN** is 20.3 kDa with a PDI of 2.79.

PT-2CN. To a mixture of compound **M1** (80 mg, 0.10 mmol), compound **M3** (3.35 mg, 0.01 mmol), compound **T-Sn** (47.01 mg, 0.11 mmol) and $Pd_2(dba)_3$ (3.15 mg, 0.003 mmol) and P(*o*-Tol)$_3$ (10.50 mg, 0.024 mmol) in a Schlenk flask was added toluene (1.5 mL) under argon. The mixture was heated to reflux for 16 h. Then the solution was cooled to room temperature and added into methanol (150 mL) dropwise. The precipitate was collected and further purified via Soxhlet extraction by using methanol, hexane, CH_2Cl_2 and $CHCl_3$ in sequence. The $CHCl_3$ fraction was concentrated and added into methanol dropwise. The precipitate was collected and dried under vacuum overnight to give **PT-2CN** (61mg, 82%). ^{1}H NMR ($CDCl_3$, 400 MHz, δ/ppm): 7.52-7.00 (br, aromatic protons), 4.27 (s, vinyl protons), 1.55-0.89 (br, aliphatic protons). M_n for **PT-2CN** is 17.7 kDa with a PDI of 3.05.

4. NMR spectra

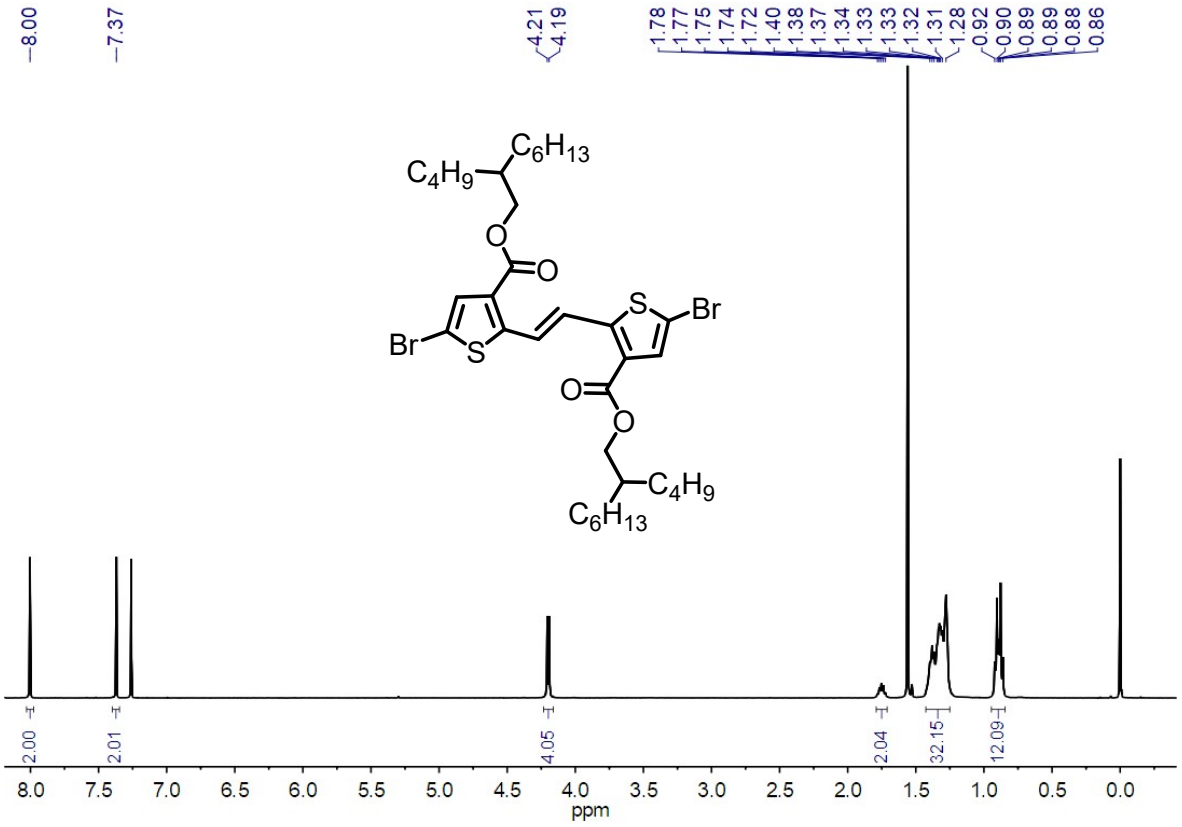

Fig. S1 ^{1}H NMR spectrum of **M1**.

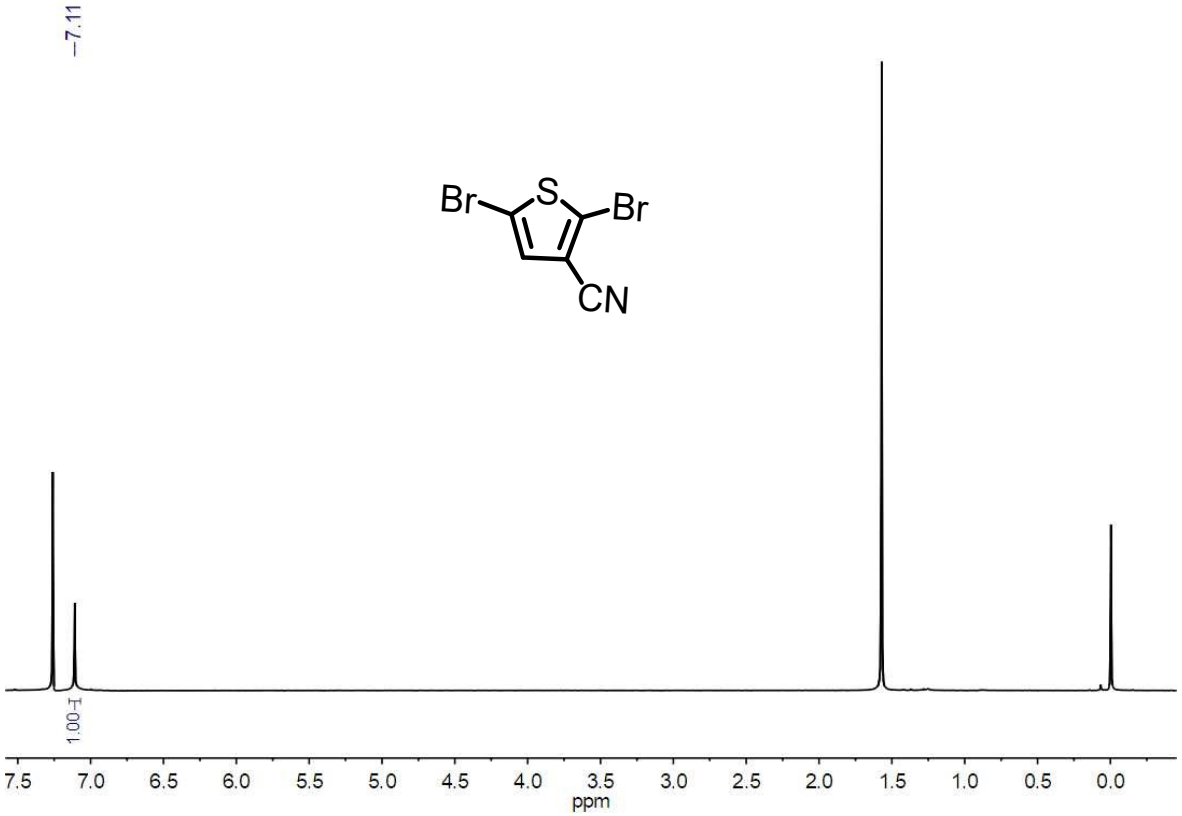

Fig. S2 ^{1}H NMR spectrum of **M2**.

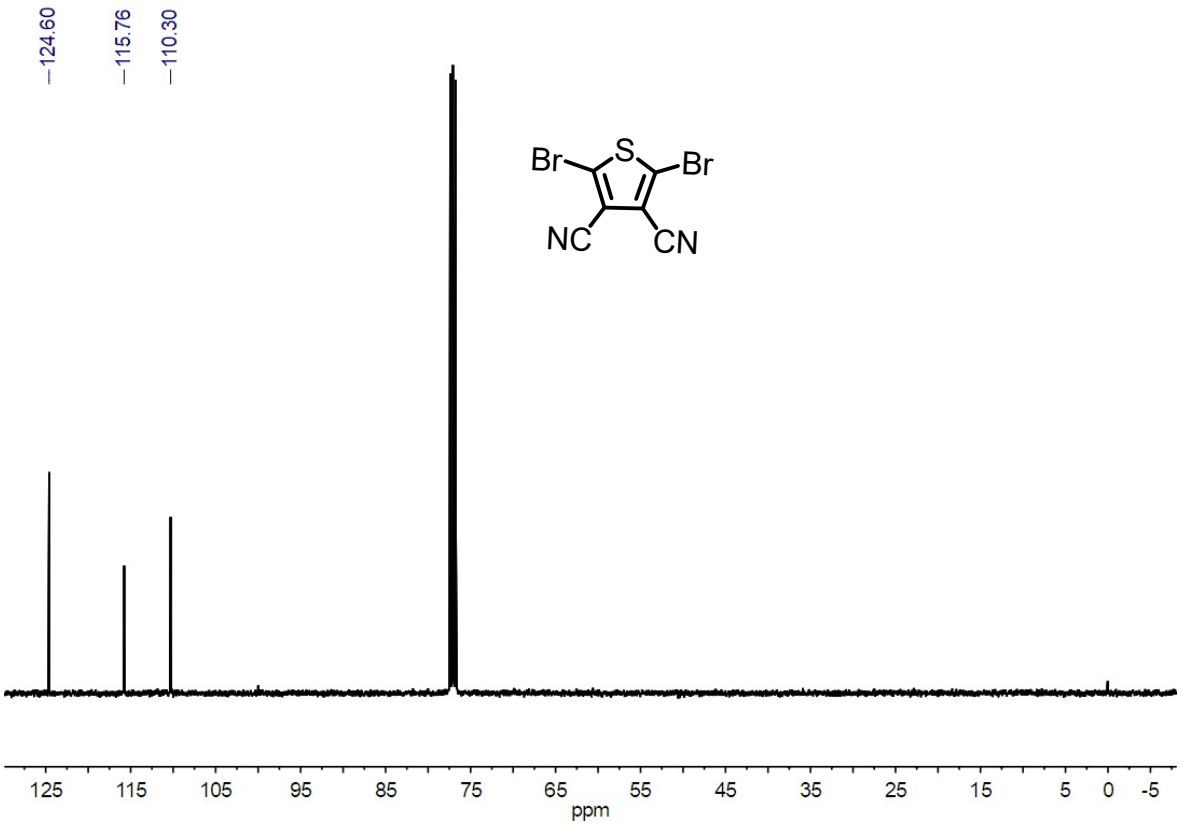

Fig. S3 ^{13}C NMR spectrum of **M3**.

5. Material cost

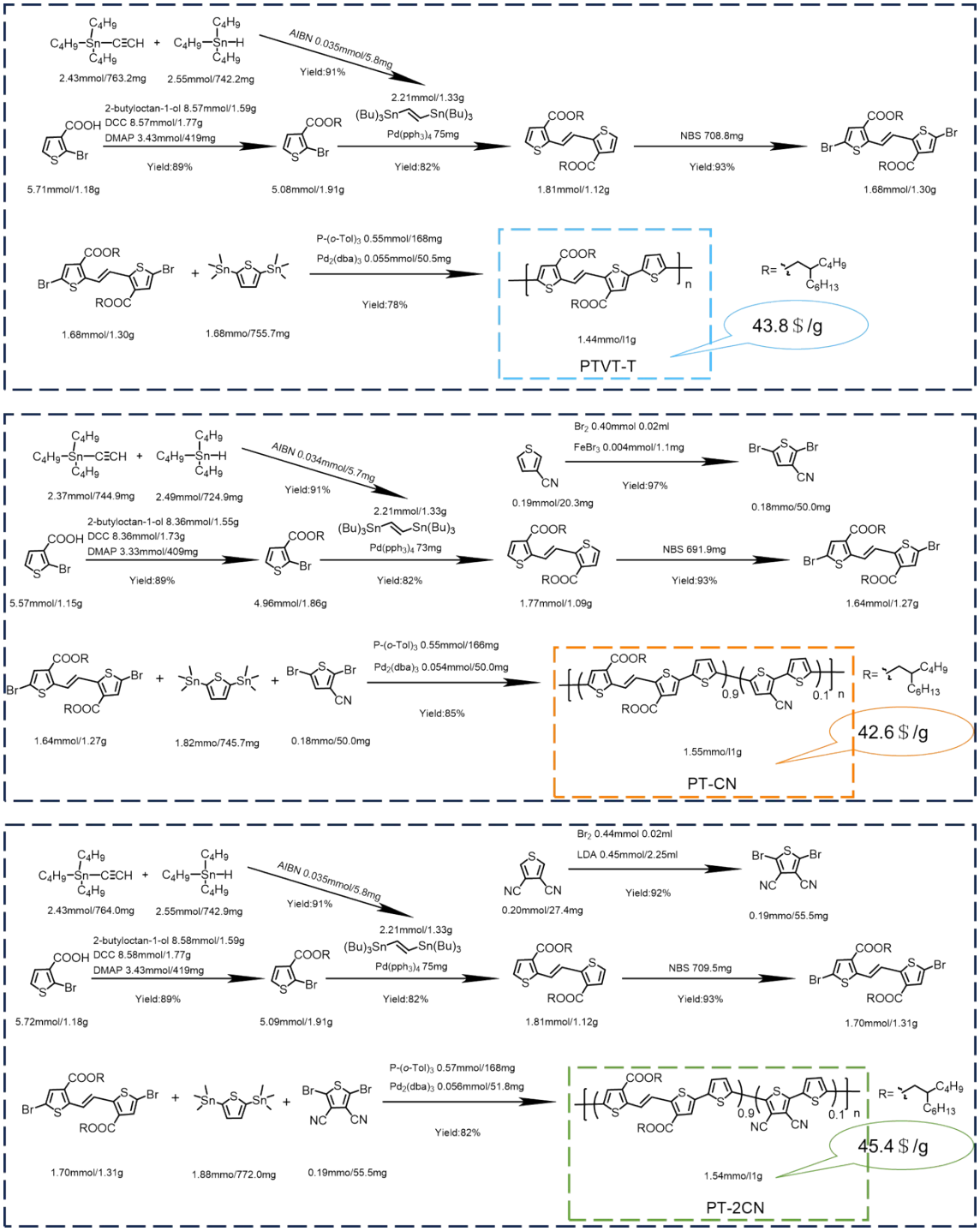

Fig. S4 Synthetic details and yields of each step of PTVT-T, PT-CN and PT-2CN.

Table S1. The material-only cost evaluation of PTVT-T, PT-CN and PT-2CN.

	PTVT-T
Donor Monomer	

Reagent	Quantity	Unit(source) (By March 2024)	Cost ($)
2,5-bis(trimethylstannyl)thiophene	755.7 mg	13.89 $/1 g(*Natl. Sci. Rev.* 2021, 8, nwab031.)	10.50
Acceptor Monomer			
Reagent	Quantity	Unit(source) (By March 2024)	Cost ($)
tributyl(ethynyl)stannane	763.2 mg	4.17 $/1 g (J&K)	3.18
AIBN	5.8 mg	5.83 $/25 g (J&K)	0.0014
tributylstannane	742.7 mg	14.59 $/10 g (J&K)	1.08
2-bromothiophene-3-carboxylic acid	1.18 g	79.46 $/5 g (J&K)	18.75
DCC	1.77 g	9.58 $/25 g (J&K)	0.68
DMAP	419 mg	6.53 $/25 g (J&K)	0.11
2-butyloctan-1-ol (ρ=0.833g/mL)	1.59 g	51.40 $/25 mL (J&K)	3.90
$Pd(PPh_3)_4$	75 mg	33.34 $/1 g (J&K)	2.50
NBS	708.7 mg	8.06 $/100 g (J&K)	0.06
Total Cost			30.66
Polymerization (1g)			
Reagent	Quantity	Unit(source) (By March 2024)	Cost ($)
$Pd_2(dba)_3$	23.08 mg	27.09 $/1 g (J&K)	1.37
P-(*o*-Tol)$_3$	168.0 mg	7.50 $/1 g (J&K)	1.26
Overall cost for 1g PTVT-T			**43.8**
PT-CN			
Donor Monomer			
Reagent	Quantity	Unit(source) (By March 2024)	Cost ($)
2,5-bis(trimethylstannyl)t	745.7 mg	13.89 $/1 g(*Natl. Sci. Rev.* 2021, 8, nwab031.)	10.36

hiophene			
Acceptor Monomer			
Reagent	Quantity	Unit(source) (By March 2024)	Cost ($)
tributyl(ethynyl)stannane	744.9 mg	4.17 $/1 g (J&K)	3.11
AIBN	5.7 mg	5.83 $/25 g (J&K)	0.0013
tributylstannane	724.9 mg	14.59 $/10 g (J&K)	1.06
2-bromothiophene-3-carboxylic acid	1.15 g	79.46 $/5 g (J&K)	18.27
DCC	1.73 g	9.58 $/25 g (J&K)	0.66
DMAP	409 mg	6.53 $/25 g (J&K)	0.11
2-butyloctan-1-ol (ρ=0.833g/mL)	1.55 g	51.40 $/25 mL (J&K)	3.83
$Pd(PPh_3)_4$	73 mg	33.34 $/1 g (J&K)	2.43
NBS	691.9 mg	8.06 $/100 g (J&K)	0.06
$FeBr_3$	1.1 mg	28.06 $/5 g (J&K)	0.006
thiophene-3-carbonitrile	20.3 mg	27.64 $/5 g (J&K)	0.11
Br_2	0.02 ml	31.95 $/500 ml (J&K)	0.001
Total Cost			29.65
Polymerization (1g)			
Reagent	Quantity	Unit(source) (By March 2024)	Cost ($)
$Pd_2(dba)_3$	50.5 mg	27.09 $/1 g (J&K)	1.37
P-(*o*-Tol)$_3$	166.0 mg	7.50 $/1 g (J&K)	1.25
Overall cost for 1g PT-CN			**42.6**
PT-2CN			
Donor Monomer			
Reagent	Quantity	Unit(source) (By March 2024)	Cost ($)
2,5-	772.0 mg	13.89 $/1 g(*Natl. Sci. Rev.* 2021,	10.72

bis(trimethylstannyl)thiophene		8, nwab031.)	
Acceptor Monomer			
Reagent	Quantity	Unit(source) (By March 2024)	Cost ($)
tributyl(ethynyl)stannane	764.0 mg	4.17 $/1 g (J&K)	3.19
AIBN	5.8 mg	5.83 $/25 g (J&K)	0.0014
tributylstannane	742.9 mg	14.59 $/10 g (J&K)	1.08
2-bromothiophene-3-carboxylic acid	1.18 g	79.46 $/5 g (J&K)	18.75
DCC	1.77 g	9.58 $/25 g (J&K)	0.68
DMAP	419 mg	6.53 $/25 g (J&K)	0.11
2-butyloctan-1-ol (ρ=0.833g/mL)	1.59 g	51.40 $/25 mL (J&K)	3.90
$Pd(PPh_3)_4$	75 mg	33.34 $/1 g (J&K)	2.90
NBS	709.5 mg	8.06 $/100 g (J&K)	0.06
thiophene-3,4-dicarbonitrile	27.4 mg	42.78 $/1 g (J&K)	1.17
LDA	2.25 ml	34.03 $/500 ml (J&K)	0.15
Br_2	0.02 ml	31.95 $/500 ml (J&K)	0.001
Total Cost			31.99
Polymerization (1g)			
Reagent	Quantity	Unit(source) (By March 2024)	Cost ($)
$Pd_2(dba)_3$	51.8 mg	27.09 $/1 g (J&K)	1.40
P-(*o*-Tol)$_3$	168.0 mg	7.50 $/1 g (J&K)	1.26
Overall cost for 1g PT-2CN			**45.4**

6. Absorption

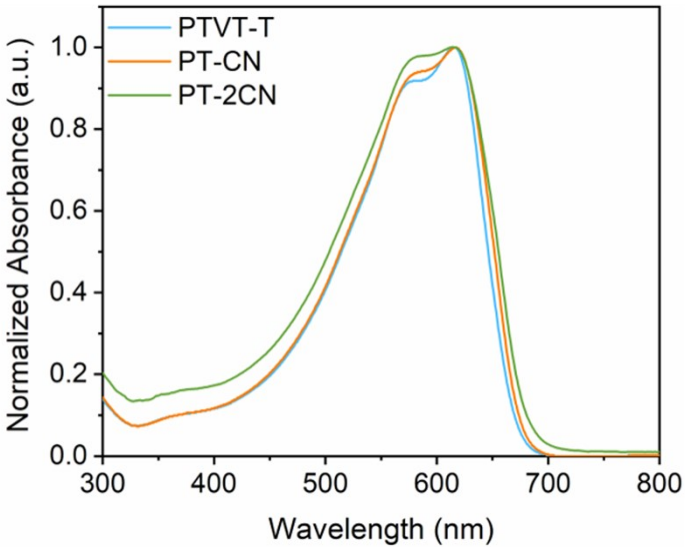

Fig. S5 Absorption spectra of PTVT-T, PT-CN and PT-2CN in $CHCl_3$ solution (10^{-5} M).

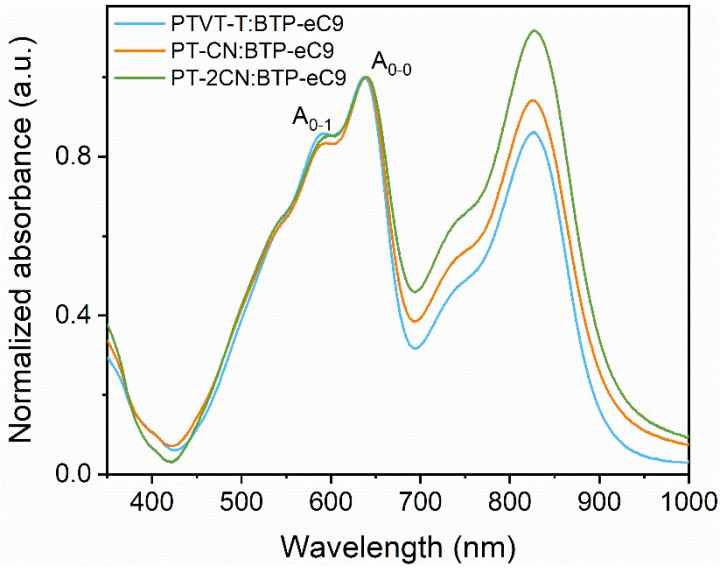

Fig. S6 Absorption spectra of PTVT-T:BTP-eC9, PT-CN:BTP-eC9 and PT-2CN:BTP-eC9 blend films.

7. Cyclic voltammetry

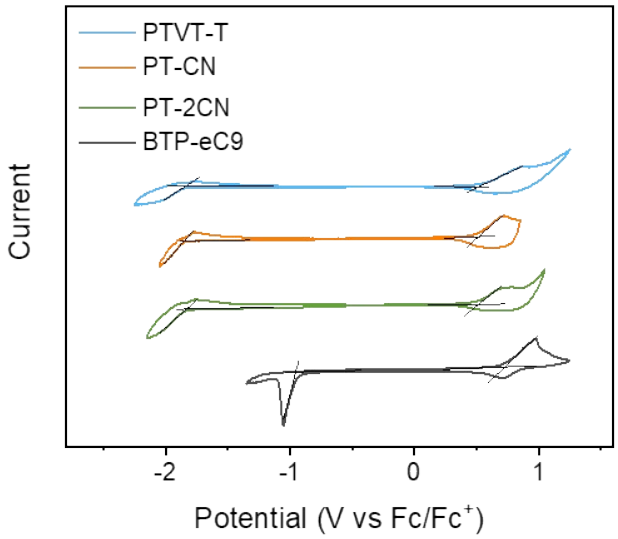

Fig. S7 Cyclic voltammograms of PTVT-T, PT-CN, PT-2CN and BTP-eC9.

Table S2. Optical and electrochemical data of PTVT-T, PT-CN, PT-2CN and BTP-eC9.

	$\lambda_{sol.}$ [nm]	λ_{film} [nm]	λ_{onset} [nm]	$^{a}E_g^{opt}$ [eV]	E_{ox}^{on} [eV]	E_{red}^{on} [eV]	HOMO [eV]	LUMO [eV]	$^{b}E_g^{ec}$ [eV]
PTVT-T	615	636	691	1.79	0.49	-1.85	-5.29	-2.95	2.34
PT-CN	617	638	693	1.79	0.51	-1.85	-5.31	-2.95	2.36
PT-2CN	615	636	695	1.78	0.52	-1.84	-5.32	-2.96	2.36
BTP-eC9	-	830	927	1.34	0.72	-0.96	-5.52	-3.84	1.68

$^{a}E_g^{opt} = 1240/\lambda_{onset}$; HOMO = -($E_{ox}^{on}$ + 4.80); LUMO = -(E_{red}^{on} + 4.80); $^{b}E_g^{ec}$ = LUMO-HOMO.

8. UPS

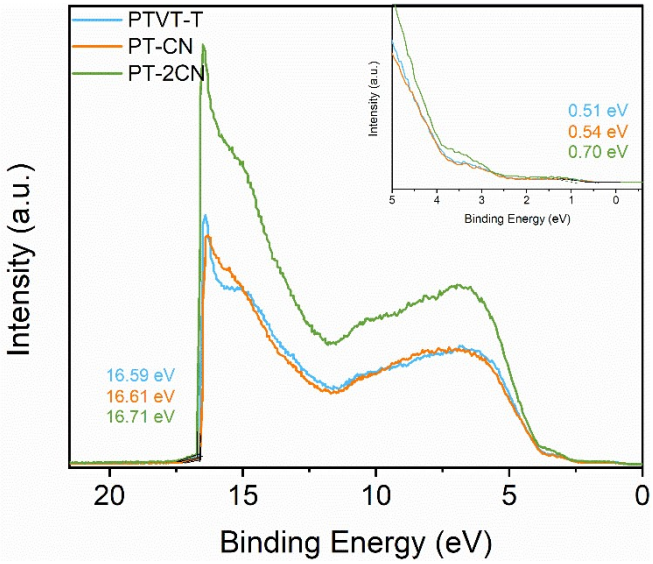

Fig. S8 UPS spectra of PTVT-T, PT-CN and PT-2CN thin films.

9. Contact angle

Contact angles of water and glycerol on polymer donors (PTVT-T, PT-CN and PT-2CN), and acceptor (BTP-eC9) neat films were measured by JY-82C contact angle analyzer. The surface tension can be evaluated by using the equation:[2]

$$\gamma_{LV}(1+cos\theta) = 4\frac{\gamma_S^d\gamma_L^d}{\gamma_S^d+\gamma_L^d} + 4\frac{\gamma_S^p\gamma_L^p}{\gamma_S^p+\gamma_L^p}$$

where γ_{LV} represents the surface tension of water/glycerol in equilibrium with its vapor. γ_L^d and γ_L^p represent the dispersion and polar components of the liquid surface tension, respectively, while γ_S^d and γ_S^p represent the dispersion and polar components of the solid surface tension, respectively. γ_S^d and γ_S^p can be calculated by using the contact angles with water and glycerol. The surface tension of donor and acceptors are calculated by equation: $\gamma = \gamma_S^d + \gamma_S^p$. The closer the surface tension, the better compatibility between two materials.

Table S3. Contact angles of water and glycerol on PTVT-T, PT-CN, PT-2CN and BTP-eC9 neat films.

	θ_{water} [°]	$\theta_{glycerol}$ [°]	γ [mN m^{-1}]	$\left(\sqrt{\gamma_{PT}}-\sqrt{\gamma_{BTP-eC9}}\right)^2$
PTVT-T	105.1	86.8	27.19	0.03
PT-CN	103.1	86.1	26.09	0.08
PT-2CN	96.6	85.7	23.38	0.31
BTP-eC9	97.4	79.6	29.08	-

10. GIWAXS

Table S4. Crystal coherence length (CCL) of π-π stacking diffraction peaks and corresponding *d*-spacings for PTVT-T, PT-CN, PT-2CN neat films, and PTVT-T:BTP-eC9, PT-CN:BTP-eC9, PT-2CN:BTP-eC9 blend films.

	q_z (Å^{-1})	*d*-spacing (Å)	FWHM (Å^{-1})	CCL (Å)
PTVT-T	1.7	3.6	0.24	23.1
PT-CN	1.7	3.6	0.25	24.3
PT-2CN	1.7	3.6	2.07	15.2
PTVT-T:BTP-eC9	1.7	3.6	0.29	19.5
PT-CN:BTP-eC9	1.7	3.6	0.26	21.7

PT-2CN:BTP-eC9	1.7	3.6	0.25	20.5

11. AFM

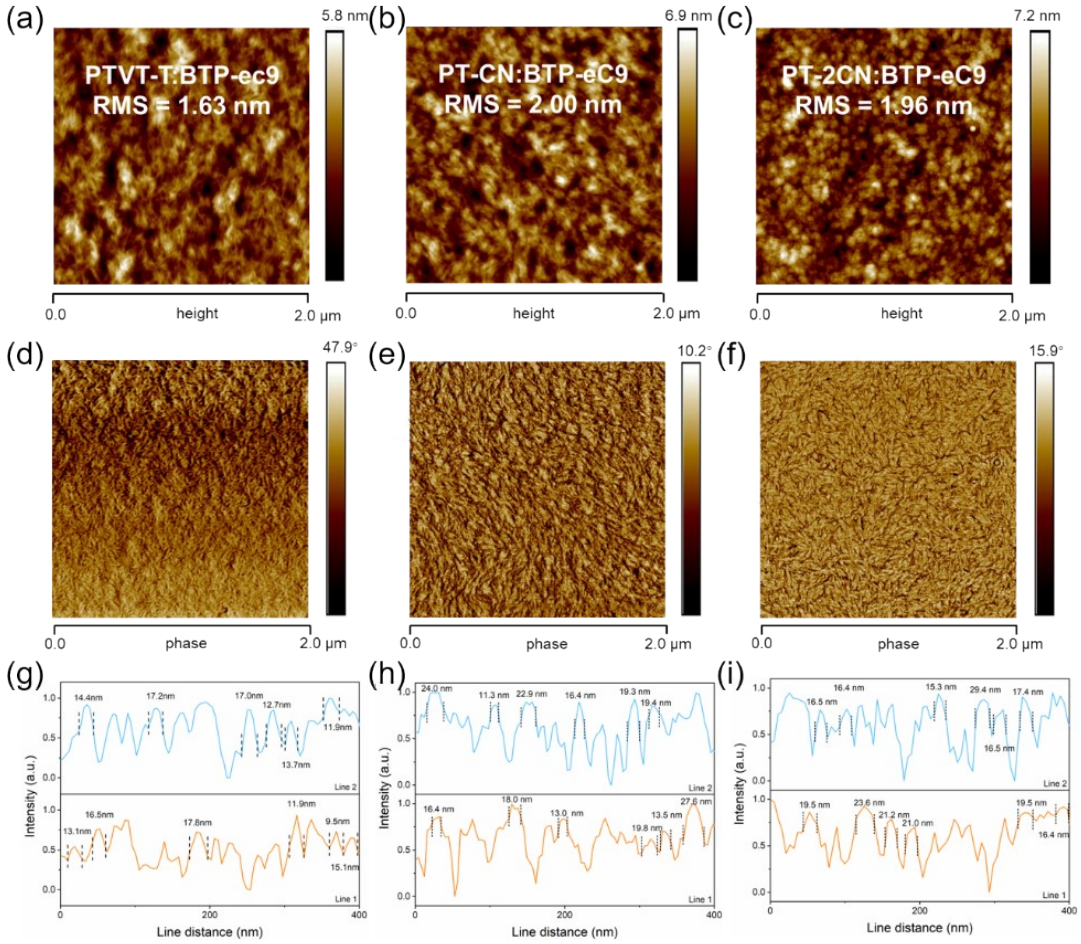

Fig. S9 AFM height images of (a) PTVT-T:BTP-eC9, (b) PT-CN:BTP-eC9 and (c) PT-2CN:BTP-eC9 blend films. AFM phase images of (d) PTVT-T:BTP-eC9, (e) PT-CN:BTP-eC9 and (f) PT-2CN:BTP-eC9 blend films. The line profiles along the white lines to obtain the fibril width of (g) PTVT-T:BTP-eC9, (h) PT-CN:BTP-eC9 and (i) PT-2CN:BTP-eC9 blend films. The fibril widths are obtained from the average FWHMs (the distance between two adjacent dashed lines in the graph).

12. Device fabrication and measurement

OSCs were fabricated with the structure of ITO/PEDOT:PSS/active layer/PDINN/Ag. The ITO glass substrates were cleaned by an ultrasonic cleaner in water with detergent, deionized water, acetone and isopropyl alcohol for 15 min successively, and subsequently treated with UV-ozone for 20 min. Then, the PEDOT:PSS layer was spin-coated onto the ITO substrate at 4000 rpm for 30 s, following by annealing under 150 °C for 10 min. PTVT-T:small molecule acceptor (SMA), PT-CN:SMA, PT-2CN:SMA blends with/without additive were dissolved in chloroform at 60 °C before spin coating, respectively. Subsequently, the solution of the blend was spin-coated onto the PEDOT:PSS layer, following by thermal annealing. Then, the electron transport layer PDINN (1.0 mg mL^{-1} in methanol) was spin-coated onto the active layer with 4000 rpm for 20 s. Finally, Ag (~100 nm) was evaporated onto the electron transport layer under vacuum (ca. 10^{-4} Pa) to form the top electrode. The effective area of the device is 0.04

cm^2.

Electron-only devices

The structure for electron-only device is ITO/ZnO/active layer/Ca/Al. The ZnO precursor was spin-coated onto the ITO glass and annealed under 200 ℃ in air for 30 min. A polythiophene:BTP-eC9 blend in $CHCl_3$ was spin-coated onto the ZnO layer. Then the film was thermally annealed in N_2. Ca (~15 nm) and Al (~60 nm) were successively evaporated onto the active layer through a shadow mask (pressure ca. 10^{-4} Pa). *J-V* characteristics were measured by using a computerized Keithley 2450 SourceMeter in the dark.

Hole-only devices

The structure for hole-only device is ITO/PEDOT:PSS/active layer/MoO_3/Ag. The PEDOT:PSS layer (~30 nm) was made by spin-coating an aqueous dispersion onto the ITO glass (4000 rpm for 30 s). The PEDOT:PSS substrates were dried under 150 °C for 10 min. A polythiophene:BTP-eC9 blend in $CHCl_3$ was spin-coated onto the PEDOT:PSS layer. Then the film was thermally annealed in N_2. Finally, MoO_3 (~3 nm) and Ag (~100 nm) was successively evaporated onto the active layer through a shadow mask (pressure ca. 10^{-4} Pa). *J-V* characteristics were measured by using a computerized Keithley 2450 SourceMeter in the dark.

Table S5. Photovoltaic parameters of representative polythiophene based OSCs in literatures.

Year	D/A	V_{OC} [V]	J_{SC} [mA cm^{-2}]	FF	PCE [%]	Ref
2015	P3HT:IDT-2BR	0.84	8.91	0.68	5.12	3
2015	P3HT:FBR	0.82	7.95	0.63	4.11	4
2016	PDCBT-2F:IT-M	1.13	10.43	0.56	6.60	5
2016	PDCBT:ITIC	0.94	16.50	0.66	10.16	6
2016	P3HT:O-IDTBR	0.72	13.90	0.60	6.30	7
2016	P3HT:EH-IDTBR	0.76	12.10	0.62	6.00	7
2017	P3HT:ATT-3	0.93	10.93	0.62	6.26	8
2017	P3HT:N6	0.90	10.78	0.63	6.11	9
2017	P3HT:H1	1.17	7.74	0.60	5.42	10
2017	P3HT:TPE-CP4	0.99	9.68	0.63	6.02	11
2017	P3HT:PCBM	0.65	11.00	0.66	4.60	12
2018	P3HT : N10	0.99	12.08	0.64	7.65	13
2018	PDCBT-2F:IT-4F	0.92	18.20	0.71	11.90	14
2018	P3HT:BTA3	0.90	9.64	0.65	5.64	15
2018	P3HT:BTDT2R	0.81	9.42	0.67	5.09	16

2018	PDCBT:IDTT-BH	0.88	17.15	0.69	10.35	17
2018	PDCBT:O-NTNC	0.94	15.51	0.66	10.00	18
2019	P4T2F-HD:O-IDTBR	1.04	10.00	0.67	7.00	19
2019	P3HT:TrBTIC	0.88	13.04	0.72	8.25	20
2019	P6T-F100:EH-IDTBR	0.99	11.20	0.66	7.3	21
2020	P3HT:ZY-4Cl	0.88	16.49	0.65	9.46	22
2020	PTOBT-Z:ITIC	0.82	19.86	0.55	9.04	23
2020	PDCBT-Cl:ITIC-Th1	0.94	18.30	0.70	12.11	24
2020	P3HT:O-IDTBR-	0.73	12.91	0.75	7.10	25
2020	P3HT:TPBT-RCN	0.81	10.29	0.61	5.11	26
2021	P4T2F-HD:Y6-BO	0.72	24.39	0.76	13.65	27
2021	P3HT:ZY-4Cl	0.89	16.50	0.65	9.60	28
2021	P3HT:ZY-4Cl	0.90	17.00	0.67	10.24	29
2021	P302:Y5	0.84	20.24	0.57	9.65	30
2021	PDCBT-Cl-Si5:ITIC-Th1	0.93	19.27	0.72	12.85	31
2021	PTVT-T:BTP-eC9	0.79	26.22	0.78	16.20	1
2022	PTVT-BT: BTP-eC9	0.79	26.75	0.77	16.31	32
2022	PTVT-V: BTP-eC9	0.77	18.89	0.47	6.77	32
2022	P3PT:ZY-4Cl	0.90	15.40	0.71	9.79	33
2022	P3HT:ZY-4Cl	0.90	17.40	17.40	10.71	34
2022	P5TCN-2F:Y6	0.85	25.07	0.75	16.10	35
2022	P5TCN-F25:Y6	0.79	27.13	0.77	16.60	36
2022	P5TCN-F25:Y6:$PC_{71}BM$	0.80	27.55	0.78	17.20	37
2023	PTTz-2FT20:m-BTP-PhC6	0.80	26.59	0.76	16.18	37
2023	PTTz-2FT20:m-BTP-PhC6 :L8-BO	0.83	26.49	0.78	17.13	37
2023	PDCBT-2F:Tz	0.88	21.1	0.72	13.30	38
2023	PT4T-2F:F8IC	0.72	21.29	0.68	10.48	39
2023	P5TCN-F25:Y6-BO	0.80	26.88	0.73	15.68	40
2024	PT-CN:BTP-eC9	0.811	27.67	0.770	17.27	***This work***

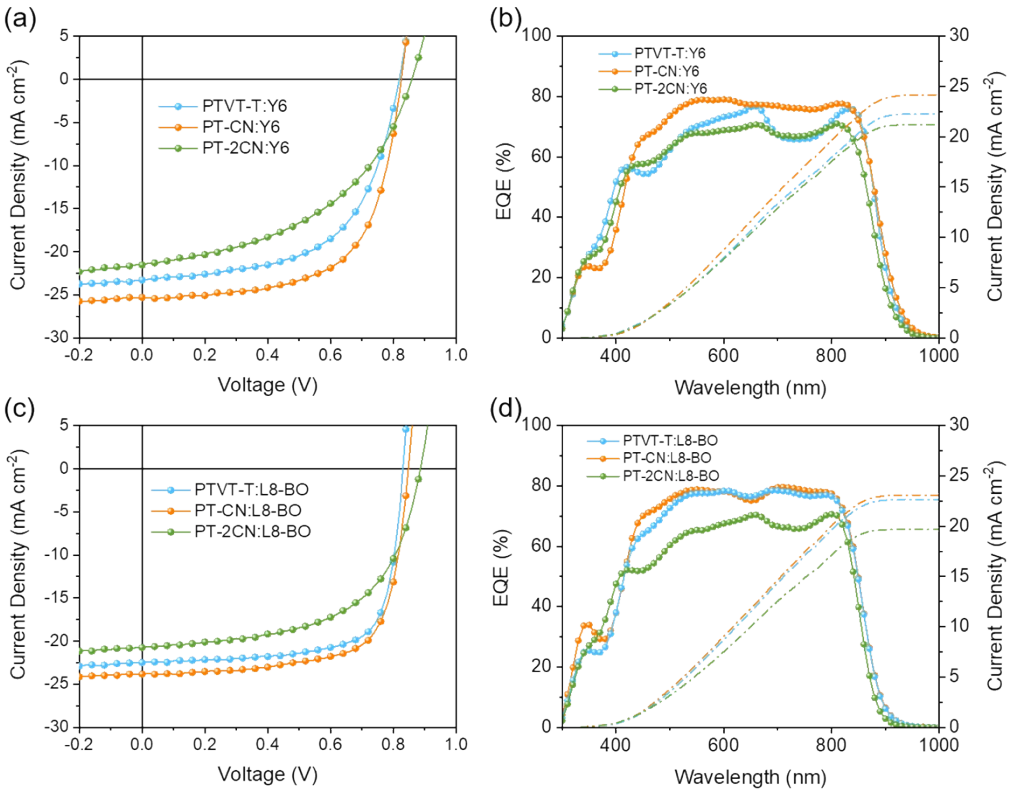

Fig. S10 (a) *J-V* curves and (b) EQE spectra of PT:Y6 based OSCs. (c) *J-V* curves and (d) EQE spectra of PT:L8-BO based OSCs.

Table S6. Photovoltaic parameters of PT:Y6 and PT:L8-BO based OSCs under AM 1.5G illumination at 100 mW cm^{-2}. The average values and standard deviations of 10 devices are shown in parentheses.

	V_{OC} [V]	J_{SC} [mA cm^{-2}]	FF [%]	PCE [%]	J_{EQE} [mA cm^{-2}]
PTVT-T:Y6	0.819 (0.818 ± 0.003)	23.27 (22.93 ± 0.42)	58.24 (57.20 ± 0.67)	11.10 (10.73 ± 0.18)	22.27
PT-CN:Y6	0.825 (0.820 ± 0.004)	25.35 (25.97 ± 0.43)	62.76 (63.91 ± 0.97)	13.37 (13.36 ± 0.14)	24.16
PT-2CN:Y6	0.859 (0.858 ± 0.004)	21.47 (21.61 ± 0.13)	47.07 (45.20 ± 1.91)	8.68 (8.38 ± 0.35)	21.21
PTVT-T:L8-BO	0.830 (0.828 ± 0.002)	22.47 (22.22 ± 0.17)	73.04 (72.83 ± 0.51)	13.63 (13.41 ± 0.14)	22.64
PT-CN:L8-BO	0.847 (0.843 ± 0.003)	23.81 (23.65 ± 0.24)	71.04 (71.28 ± 1.01)	14.34 (14.22 ± 0.23)	23.07
PT-2CN:L8-BO	0.886 (0.888 ± 0.005)	20.74 (20.72 ± 0.70)	57.96 (57.55 ± 2.13)	10.65 (10.58 ± 0.22)	19.67

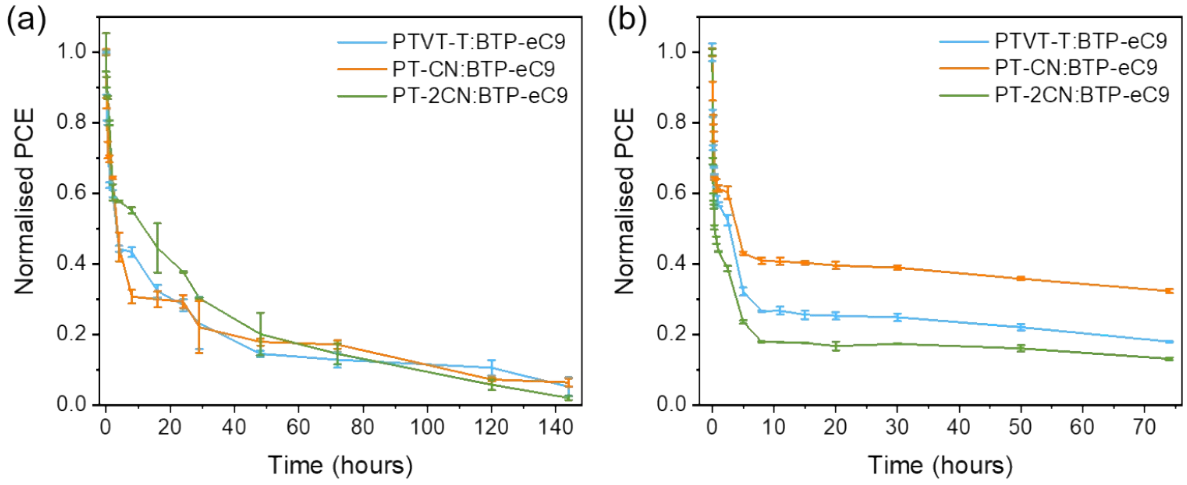

Fig. S11 Normalized PCEs of PT:BTP-eC9 based OSCs after long-term (a) light soaking under two-sun intensity illumination in air and (b) thermal annealing under 85 °C under nitrogen in the glove box.

13. SCLC

Charge carrier mobility was obtained by using the SCLC method. The mobility was determined by fitting the dark current to the model of a single carrier SCLC, which is described by:

$$J = \frac{9}{8}\varepsilon_0\varepsilon_r\mu\frac{V^2}{d^3}$$

where J is the current density, μ is the zero-field mobility of electron (μ_e) or hole (μ_h), ε_0 is the permittivity of the vacuum, ε_r is the relative permittivity of the material, d is the thickness of the active layer, and V is the effective voltage, $V = V_{appl} - V_{bi}$ (V_{appl} is the applied voltage, and V_{bi} is the built-in potential determined by the electrode work function difference.).

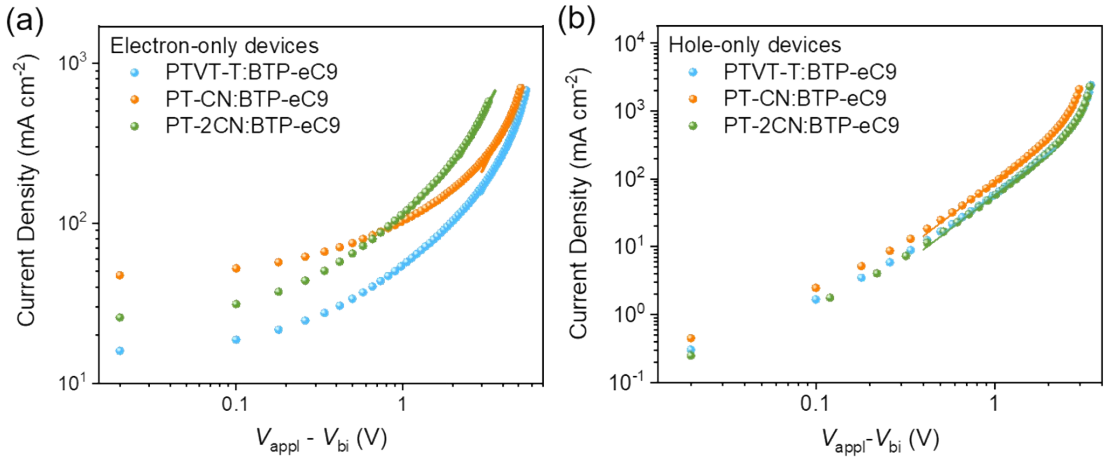

Fig. S12 Typical current density-applied voltage log plots for (a) electron-only devices and (b) hole-only devices based on PTVT-T:BTP-eC9, PT-CN:BTP-eC9 and PT-2CN:BTP-eC9 blend

films under dark. The measured data are shown as symbols, while the solid lines are the best fits to the SCLC model. Mobilities were extracted from the fitting.

Table S7. Charge carrier mobilities of PTVT-T:BTP-eC9, PT-CN:BTP-eC9 and PT-2CN:BTP-eC9 based devices via SCLC method.

	μ_e (10^{-4} cm^2 V^{-1} s^{-1})	μ_h (10^{-4} cm^2 V^{-1} s^{-1})
PTVT-T:BTP-eC9	1.76	7.92
PT-CN:BTP-eC9	3.06	11.10
PT-2CN:BTP-eC9	2.33	3.33

References

1. J. Ren, P. Bi, J. Zhang, J. Liu, J. Wang, Y. Xu, Z. Wei, S. Zhang and J. Hou, *Natl. Sci. Rev.*, 2021, **8**, nwab031.
2. J. Comyn, *Int. J. Adhes. Adhes.*, 1992, **12**, 145-149.
3. Y. Wu, H. Bai, Z. Wang, P. Cheng, S. Zhu, Y. Wang, W. Ma and X. Zhan, *Energy Environ. Sci.*, 2015, **8**, 3215-3221.
4. S. Holliday, R. S. Ashraf, C. B. Nielsen, M. Kirkus, J. A. Röhr, C.-H. Tan, E. Collado-Fregoso, A.-C. Knall, J. R. Durrant, J. Nelson and I. McCulloch, *J. Am. Chem. Soc.*, 2015, **137**, 898-904.
5. H. Zhang, S. Li, B. Xu, H. Yao, B. Yang and J. Hou, *J. Mater. Chem. A*, 2016, **4**, 18043-18049.
6. Y. Qin, M. A. Uddin, Y. Chen, B. Jang, K. Zhao, Z. Zheng, R. Yu, T. J. Shin, H. Y. Woo and J. Hou, *Adv. Mater.*, 2016, **28**, 9416-9422.
7. S. Holliday, R. S. Ashraf, A. Wadsworth, D. Baran, S. A. Yousaf, C. B. Nielsen, C.-H. Tan, S. D. Dimitrov, Z. Shang, N. Gasparini, M. Alamoudi, F. Laquai, C. J. Brabec, A. Salleo, J. R. Durrant and I. McCulloch, *Nat. Commun.*, 2016, **7**, 11585.
8. F. Liu, J. Zhang, Z. Zhou, J. Zhang, Z. Wei and X. Zhu, *J. Mater. Chem. A*, 2017, **5**, 16573-16579.
9. D. Srivani, A. Agarwal, S. V. Bhosale, A. L. Puyad, W. Xiang, R. A. Evans, A. Gupta and S. V. Bhosale, *Chem. Commun.*, 2017, **53**, 11157-11160.
10. A. Gupta, A. Rananaware, P. S. Rao, D. D. La, A. Bilic, W. Xiang, J. Li, R. A. Evans, S. V. Bhosale and S. V. Bhosale, *Mater. Chem. Front.*, 2017, **1**, 1600-1606.
11. A. Rananaware, A. Gupta, G. Kadam, D. D. La, A. Bilic, W. Xiang, R. A. Evans and S. V. Bhosale, *Mater. Chem. Front.*, 2017, **1**, 2511-2518.
12. H. Park, B. Jin, Y. Kim, C. Im, J. An, H. Park and W. Tian, *J. Korean Phy. Soc.*, 2017, **70**, 177-183.
13. P. S. Rao, A. Gupta, D. Srivani, S. V. Bhosale, A. Bilic, J. Li, W. Xiang, R. A. Evans and S. V. Bhosale, *Chem. Commun.*, 2018, **54**, 5062-5065.
14. H. Yao, D. Qian, H. Zhang, Y. Qin, B. Xu, Y. Cui, R. Yu, F. Gao and J. Hou, *Chin. J. Chem.*, 2018, **36**, 491-494.

15. B. Xiao, A. Tang, Q. Zhang, G. Li, X. Wang and E. Zhou, *ACS Appl. Mater. Interfaces*, 2018, **10**, 34427-34434.
16. J. Ahn, S. Oh, H. Lee, S. Lee, C. E. Song, H. K. Lee, S. K. Lee, W.-W. So, S.-J. Moon, E. Lim, W. S. Shin and J.-C. Lee, *ACS Appl. Mater. Interfaces*, 2019, **11**, 30098-30107.
17. M. Chang, Y. Wang, Y.-Q.-Q. Yi, X. Ke, X. Wan, C. Li and Y. Chen, *J. Mater. Chem. A*, 2018, **6**, 8586-8594.
18. H. Feng, Y.-Q.-Q. Yi, X. Ke, Y. Zhang, X. Wan, C. Li and Y. Chen, *Solar RRL*, 2018, **2**, 1800053.
19. X. Jia, Z. Chen, C. Duan, Z. Wang, Q. Yin, F. Huang and Y. Cao, J. Mater. Chem. C, 2019, 7, 314-323.
20. X. Xu, G. Zhang, L. Yu, R. Li and Q. Peng, *Adv. Mater.*, 2019, **31**, 1906045.
21. X. Jia, G. Liu, S. Chen, Z. Li, Z. Wang, Q. Yin, H.-L. Yip, C. Yang, C. Duan, F. Huang and Y. Cao, *ACS Appl. Energy Mater.*, 2019, **2**, 7572-7583.
22. C. Yang, S. Zhang, J. Ren, M. Gao, P. Bi, L. Ye and J. Hou, *Energy Environ. Sci.*, 2020, **13**, 2864-2869.
23. K. He, P. Kumar, M. Abd-Ellah, H. Liu, X. Li, Z. Zhang, J. Wang and Y. Li, *Macromolecules*, 2020, **53**, 8796-8808.
24. Z. Liang, M. Li, Q. Wang, Y. Qin, S. J. Stuard, Z. Peng, Y. Deng, H. Ade, L. Ye and Y. Geng, *Joule*, 2020, **4**, 1278-1295.
25. K. An, W. Zhong and L. Ying, *Org. Electron.*, 2020, **82**, 105701.
26. J. Yang, Y. Geng, J. Li, B. Zhao, Q. Guo and E. Zhou, *J. Phy. Chem. C*, 2020, **124**, 24616-24623.
27. J. Xiao, X. Jia, C. Duan, F. Huang, H.-L. Yip and Y. Cao, *Adv. Mater.*, 2021, **33**, 2008158.
28. Y. Liu, K. Xian, Z. Peng, M. Gao, Y. Shi, Y. Deng, Y. Geng and L. Ye, *J. Mater. Chem. A*, 2021, **9**, 19874-19885.
29. C. Yang, R. Yu, C. Liu, H. Li, S. Zhang and J. Hou, *ChemSusChem*, 2021, **14**, 3607-3613.
30. C. Yang, S. Zhang, J. Ren, P. Bi, X. Yuan and J. Hou, *Chin. Chem. Lett.*, 2021, **32**, 2274-2278.
31. Q. Wang, M. Li, Z. Peng, N. Kirby, Y. Deng, L. Ye and Y. Geng, *Sci. China Chem.*, 2021, **64**, 478-487.
32. P. Bi, J. Ren, S. Zhang, J. Wang, Z. Chen, M. Gao, Y. Cui, T. Zhang, J. Qin, Z. Zheng, L. Ye, X. Hao and J. Hou, *Nano Energy*, 2022, **100**, 107463.
33. X. Yang, M. Gao, Z. Bi, Y. Liu, K. Xian, Z. Peng, Q. Qi, S. Li, J. Song, W. Ma and L. Ye, *Macromol. Rapid Commun.*, 2022, **43**, 2200229.
34. K. Xian, Y. Liu, J. Liu, J. Yu, Y. Xing, Z. Peng, K. Zhou, M. Gao, W. Zhao, G. Lu, J. Zhang, J. Hou, Y. Geng and L. Ye, *J. Mater. Chem. A*, 2022, **10**, 3418-3429.
35. X. Yuan, Y. Zhao, Y. Zhang, D. Xie, W. Deng, J. Li, H. Wu, C. Duan, F. Huang and Y. Cao, *Adv. Funct. Mater.*, 2022, **32**, 2201142.
36. X. Yuan, Y. Zhao, D. Xie, L. Pan, X. Liu, C. Duan, F. Huang and Y. Cao, *Joule*, 2022, **6**, 647-661.
37. H. Ma, Z. Sun, M. Jeong, S. Yang, S. Jeong, S. Lee, Y. Cho, J. Park, J. Park and C. Yang,

Chem. Eng. J., 2023, **474**, 145531.
38. Z. Li, H. Yao, L. Ma, J. Wang, Z. Bi, S. Wang, S. Seibt, T. Zhang, Y. Xu, J. Ren, Y. Xiao, C. An, W. Ma and J. Hou, *Adv. Funct. Mater.*, 2023, **33**, 2300202.
39. J. He, Z. Liang, L. Lin, S. Liang, J. Xu, W. Ni, M. Li and Y. Geng, *Polymer*, 2023, **274**, 125890.
40. X. Tan, Y. Li, X. Yuan, S. Kim, Y. Zhang, C. Yang, F. Huang, Y. Cao and C. Duan, *Sci. China Chem.*, 2023, **66**, 2347-2353.